Experimental Investigation of Seismically Resistant Bridge Piers under Blast Loading

Shuichi Fujikura[1] and Michel Bruneau, F.ASCE[2]

Abstract: This paper reports the findings of research examining the blast resistance of bridge piers that are designed in accordance with current knowledge and specifications to ensure ductile seismic performance. Blast testing was conducted on 1/4 scale ductile RC columns, and nonductile RC columns retrofitted with steel jacketing. The seismically designed RC and steel jacketed RC columns did not exhibit a ductile behavior under blast loading and failed in shear at their base rather than flexural yielding. A moment-direct shear interaction model was proposed to account for the reduction of direct shear resistance on cross sections when large moments are simultaneously applied. This made it possible to match and explain the experimentally obtained behavior when direct shear strength was compared with the shear demand obtained from plastic analysis.

Introduction

The United States has not suffered from sustained terrorist campaigns like other countries (Jenkins 2001). However, as seen in recent terrorist attacks in the United States such as the Alfred P. Murrah Federal Building bombing in 1995 and the September 11, 2001 attacks (9/11), the terrorist threat in the United States is real. Following the aftermath of 9/11, government leaders, infrastructure owners and the engineering community have recognized that the nation's highway system has vulnerabilities and collapse of a critical bridge could result in tremendous casualties and enormous economic loss. This resulted in the recent publication of a number of documents addressing this concern [see, for instance, Federal Highway Administration (FHWA) 2003; Anwarul Islam and Yazdani 2006; Ray 2006; ASCE 2008; Winget et al. 2008; Agrawal et al. 2009; Williamson and Williams 2009; Davis et al. 2009; Yi 2009; and others summarized in Fujikura and Bruneau 2008].

Bridges are exposed to multiple hazards beyond terrorist focused issues alone. To better integrate these diverse threats with conflicting demands on structural systems, there has been a growing trend in the engineering community to find integrated solutions for the design of infrastructures across various hazards, namely multihazard engineering. Multihazard engineering is here defined as the search for a single design concept which can satisfactorily fulfill the demands of multiple hazards. The properties that might be desirable to resist one hazard may have detrimental effects to resist other hazards. Therefore, multihazard engineering addresses problems of infrastructures from the system perspective by establishing optimized solutions that can provide protections against multiple hazards (e.g., Agrawal et al. 2009).

The writers previously presented the development and experimental validation of a multihazard bridge pier concept, i.e., a bridge pier system capable of providing an adequate level of protection against collapse under both seismic and blast loading (Fujikura et al. 2007, 2008). The proposed concept was a multi-column pier bent with concrete-filled steel tube (CFST) columns that could provide ductile behavior up to 7% drift under seismic excitations and approximately 20% drift under blast loading (Marson and Bruneau 2004; Fujikura et al. 2007). The columns turned out to be effective for blast loadings because breaching and spalling of concrete are prevented in CFST columns.

While CFST columns perform excellent in a multihazard perspective, they have not been commonly used in bridge engineering practice. Questions arose as to whether conventional columns designed to perform satisfactory under seismic excitations would possess adequate blast resistance. RC has been widely used for bridge columns, and seismic detailing requirements for RC columns that can behave in a ductile manner during earthquakes are provided by various documents, such as those published by the AASHTO and the California Department of Transportation (CALTRANS). Furthermore, in many parts of the United States, particularly in California, reinforcement detailing requirements in effect prior to the 1971 San Fernando earthquake resulted in RC columns that exhibited nonductile behavior during earthquakes. Many methods have been used to retrofit such nonductile columns. One of the most popular methods is steel jacketing which has been commonly used on the west coast of the United States. A column retrofitted with a steel jacket visually resembles a CFST column, but is typically discontinuous at the column top and base in order to avoid undesirable overload of the adjacent members (i.e., footing or cap beam) due to composite action that would significantly increase the flexural strength of the column (Buckle et al. 2006).

Therefore, the objective of the research presented here was to

[1]Structural Engineer, Buildings Sector, Arup North America, Los Angeles, CA 90066. E-mail: shuichi.fujikura@arup.com
[2]Professor, Dept. of Civil, Structural, and Environmental Engineering, Univ. at Buffalo, Buffalo, NY 14260. E-mail: bruneau@buffalo.edu
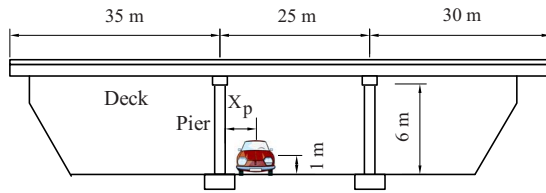
Fig. 1. Schematics of prototype bridge and assumed blast scenario

investigate the blast resistance of commonly used bridge columns, namely seismically ductile RC columns and nonductile RC columns retrofitted with steel jackets to make them ductile, detailed in accordance to recent codes of practice. This paper reports the experimental and analytical investigation of these two types of columns under blast loading. This test series also complements the first series of CFST columns testing under blast loading by Fujikura et al. (2007, 2008). Note that the assumed blast scenario is the detonation of explosives located inside a small vehicle below the bridge deck at close distance to the column, which, for comparison purposes, is the same as the one for the CFST column tests [see Fujikura et al. 2007, 2008 for details].

Seismic Design of Prototype Bridge Pier Bent

Target Bridge Structure and Analysis for Seismic Load

The target prototype bridge pier bents are part of a typical three-span continuous highway bridge, as illustrated in Fig. 1, that was used for the first series of CFST column tests (Fujikura et al. 2007, 2008). The total length is 90 m, and the span lengths are 35, 25, and 30 m. The width of the deck is 16 m, the cross-sectional area of the deck is 0.592 m^2, the moment of inertia of the transformed deck section (with respect to a vertical axis passing through the centroid) is $I_D = 13.9$ m^4, the mass of the deck per unit length is $m_D = 12.56$ t/m. Each pier bent consists of three columns with height of 6 m, a cap beam and a foundation beam. The total gravity load on each bent is assumed equal to 4,098 kN.

Response spectrum analyses were conducted for this prototype bridge. The bridge was assumed to be located in an area of moderate seismic activity and to be constructed on rock or very stiff soil foundations. The pseudoacceleration (S_A) response spectrum used for the analyses was the same as the one used for the CFST column design with the peak acceleration of 2.50 A_g (peak ground acceleration, $A_g = 0.3$ g) varying as a function of $1/T$ in the long period range. The analyses of bent columns for seismic loading were made independently in the longitudinal and transverse directions. Stiffness and strength in both directions are assumed to be provided by the piers alone as the bearings at the abutments do not restrain displacement. The inertia forces from the superstructure are assumed to be equally carried by two pier bents.

In the analyses, an axial force-moment interaction curve for the RC columns was calculated using XTRACT (XTRACT Educational Version, ver. 3.0.8, TRC/Imbsen Software Systems, Rancho Cordova, Calif., 2007). The specified concrete compressive strength, f'_c, and longitudinal and transverse steel yield stress, f_y, were set to be 27.6 MPa (4 ksi) and 414 MPa (60 ksi), respectively. A column diameter of 813 mm (32 in.) was selected to achieve an axial load level that would be about 10% of $A_g f'_c$; the actual resulting axial load level, $P/A_g f'_c$, was 11%. The column was reinforced with 16-D19 (#6) longitudinal bars, resulting in a longitudinal reinforcement ratio, ρ_l, of 0.9%. The Mander model

(Mander et al. 1988; Priestley et al. 1996) was selected for the constitutive relationship of unconfined and confined concrete. In the confined concrete model, D16 (#5) transverse spiral reinforcement was used at a spacing of 114 mm (4.5 in.). These spiral details were determined from the seismic design presented later. The resulting ductility demands in the longitudinal and transverse direction were 2.22 and 3.39, respectively. The calculations showed that the reinforced concrete bent column with diameter of 813 mm (32 in.) and 16-D19 (#6) longitudinal bars provided satisfactory performance for the considered seismic loading.

Design of Ductile RC Columns

Generally, the ductile energy dissipating elements in bridges are the columns. Nonductile failure of the columns, such as shear failure, needs to be avoided to achieve this ductile energy dissipation through inelastic flexural response of the columns. The rest of the structure has to be designed to remain elastic for the forces developed when the columns yield. This is consistent with capacity design principles. To ensure that the columns do not fail in shear prior to the development of ductile flexural hinges, the flexural capacity of the columns is magnified by an overstrength factor accounting for the increase in strength that can be developed by strain hardening and other causes. This overstrength factor was taken as 1.5 to calculate the shear demand in each column, V_u (MCEER/ATC-49 2003).

Three different design codes or guidelines for bridges, namely AASHTO (2004), MCEER/ATC-49 (2003), and California Department of Transportation (CALTRANS) (2003, 2006), were used for design of the prototype bridge pier bent. The columns were designed to be in compliance with all three (although differences were small, the more stringent requirements were taken as governing in all cases). Note that to calculate the shear resistance of the columns, MCEER/ATC-49 considers the contribution of shear resistance from transverse reinforcement, strut action and concrete tensile strength, while AASHTO does not consider the strut action in these three contributions. The plastic hinge region of the columns was detailed to achieve ductile seismic behavior of the columns. Transverse reinforcement ratio of 0.98% was provided in the plastic hinge region, which is based on the spacing of six times the nominal diameter of longitudinal reinforcement (by CALTRANS and MCEER/ATC-49). Therefore, in the plastic hinge region, D16 (#5) transverse spiral reinforcement was used at a spacing of 114 mm (4.5 in.). The length of this plastic hinge zone, L_p, was taken as 1.0 m (39 in.), which is one sixth the height of the column in accordance with AASHTO (2004).

Design of Steel Jacketed Nonductile RC Columns

The second type of seismically designed columns considered is the nonductile RC column retrofitted with a steel jacket. The steel jacket is effective to enhance the ductility of nonductile reinforced concrete columns by adding a steel shell that provides confinement to the concrete. This steel jacket allows plastic hinges to develop at the top and bottom of the column where such plastic hinges would be unable to form in a nonductile column without adequate transverse reinforcement. The same column diameter and longitudinal reinforcement as provided in the ductile RC columns were selected for the nonductile RC columns, namely 813 mm (32 in.) and 16-D19 (#6) longitudinal bars, respectively. Then, regular transverse reinforcement was designed simply to resist the shear force. The D13 (#4) transverse spiral
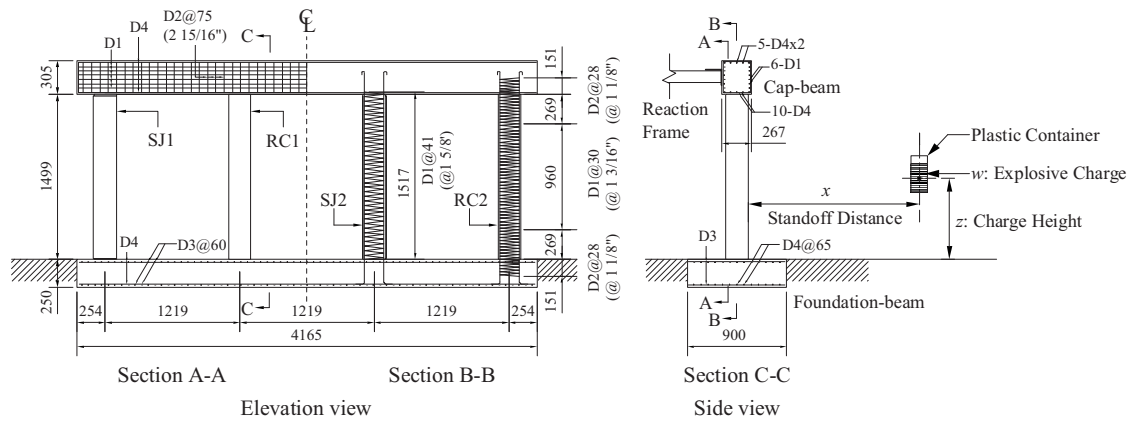
Fig. 2. Experimental specimen and explosive charge scenario

reinforcement was provided, spaced at 210 mm (8 1/4 in.), resulting in a transverse reinforcement ratio of 0.35%.

Then, this nonductile RC column was retrofitted using a steel jacket in accordance with the design procedure developed by Chai et al. (1991) (as reported in Buckle et al. 2006). In this procedure, for a circular column, the required steel jacket thickness, t, could be obtained from equilibrium of stress action on a half-column section by the following equation:

$$t \geq \frac{f_l D}{2f_s} \tag{1}$$

where f_l=confinement stress; D=diameter of column; and f_s =stress induced in the steel jacket (Buckle et al. 2006). A clearance of 13 mm (1/2 in.) provided between the existing column and the steel jacket was grouted. The confinement stress, f_l, was taken as 2.07 MPa (300 psi), as recommended in the design procedure developed by Chai et al. (1991). The stress induced in the steel jacket, f_s, was taken as 200 MPa (29 ksi) that is the stress at a strain of 0.001 calculated using a elastic modulus equal to 200 GPa (29,000 ksi). The resulting thickness of the steel jacket was 4.3 mm (3/16 in.).

One-Fourth Scale Experimental Specimens

Design of Specimens

Using geometric similitude, a one-fourth (1/4) scale model was designed and constructed to accommodate the constraints in the maximum possible explosive weight that could be used at the test site and considerations for construction cost. The bent of experimental specimen is shown in Fig. 2 along with an explosive charge scenario. The bent consists of two identical RC columns

(RC1 and RC2) and two identical steel jacketed RC columns (SJ1 and SJ2), connected to a cap beam and a footing. Note that the prototype bridge pier bent has three columns while the specimen had four columns. This was intended to provide as many columns as possible in one bent, while at the same time providing some distance between the columns needed to avoid the blast effects from a test on one column to impact the other column tests. Preliminary calculations indicated that the spacing between these columns was adequate to preclude the damage to adjacent columns by a test on a target specimen.

Materials

The concrete mix was designed to provide a 28 day target compressive strength of 4 ksi (27.6 MPa), slump of 4.5 in. (114 mm) and maximum size of coarse aggregate of 1/2 in. (13 mm). The concrete was poured in two stages; first to build the footing and second to construct the columns and cap beam. At the concrete joints between the footing and the columns, the surface of the joints was cleaned and laitance was removed in accordance with the ACI code requirement [American Concrete Institute (ACI) 2004]. The compressive strength of the concrete was obtained from compression tests of concrete cylinders with 4 in. (102 mm) diameter and 8 in. (203 mm) height. Average compressive concrete cylinder strengths at 6 days after blast tests were 41.5 MPa (6.0 ksi) for a footing and 32.1 MPa (4.7 ksi) for a cap beam and columns (61 and 41 days, respectively, after casting concrete), which are the properties that were used for the analytical study reported later in this paper (modified by factors to account for strain rate effects described later).

In the design of the prototype bridge, D13 (#4), D16 (#5), D19 (#6), and D22 (#7) deformed reinforcing bars with specified yield strength of 414 MPa (60 ksi) were used. According to geometric

Table 1. Mechanical Properties of Prototype Bridge and 1/4 Scale Model Reinforcing Bars

Prototype bridge		1/4 scale model			
Deformed reinforcing bar size	Cross-sectional area (mm²)	Deformed wire size	Cross-sectional area (mm²)	Yield strength (MPa)	Young's modulus (MPa)
D13 (#4)	126.7	D-1	6.5	380	194,289
D16 (#5)	198.6	D-2	12.9	314	193,269
D19 (#6)	286.5	D-3	19.4	501	195,007
D22 (#7)	387.2	D-4	25.8	N/A	N/A

Note: N/A=not applicable.
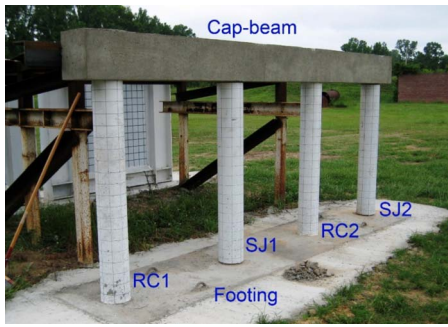
Fig. 3. Test setup from front diagonal view

similitude at one-quarter scale, D-1, D-2, D-3, and D-4 deformed steel wires were used to, respectively, model the D13, D16, D19, and D22 of the prototype bridge as shown in Table 1. These are cold-formed deformed steel wires intended for use as reinforcement in concrete construction specified by ASTM A496. The steel wires typically have high strength with no plateau and low ductility. Therefore, the steel wires used in the specimens were heat treated (annealed) to achieve properties similar to those of commercial steel reinforcing bars with design yield strength of 414 MPa (60 ksi). This was done for the D-1, D-2, and D-3 wires used to fabricate the column reinforcement. Heat treatment of the reinforcement used in the cap beam and footing was not accomplished since these structural elements were designed to remain undamaged during this experimental program and were not the focus of this research. The steel wires were placed in a vacuum furnace at room temperature, heated to 613°C (1135°F) for 60 min, cooled to room temperature, and removed. The measured yield strengths and Young's moduli of the annealed steel wires are presented in Table 1.

The steel plate for the steel jacket was specified to be ASTM 1008 CS steel. The measured thickness of the plate was 1.13 mm (0.0445 in.). The mean values of measured yield strength and Young's modulus were 254 and 207,216 MPa, respectively.

Test Setup

The blast testing was conducted at the U.S. Army Corps of Engineers Research Facility in Vicksburg, Mississippi. The experimental setup is shown in Fig. 3. The model was placed by casting concrete around the footing, as shown in this figure. The bent was braced in what would correspond to the bridge longitudinal direction at the level of the cap beam. Note that the cap beam was not connected to the frame but in contact with the frame, such as to support the horizontal force from the cap beam. Although rebound of the cap beam was not prevented by this setup, it was inconsequential given that damage to the columns here develops under pressures acting toward the reaction frames (rather than due

to oscillation of the columns). Also, note that no instrumentation (such as strain gauges and pressure transducers) was installed since it is difficult to measure data with these devices in the close-in range considered in these blast tests.

Experimental Cases

Summary of the column test cases is presented in Table 2 along with the description of test observations. Exact values of charge weights and standoff distances are not presented for security reasons; instead these values were normalized by the parameters of X and W, respectively. Three parameters were considered in deciding test conditions: height of charge, z, standoff distance, x, and weight of charge, w, as illustrated in Fig. 2. For example, when $x=X$, the stand-off distance for that test matched that for the credible threat. For $x=2.0X$, the blast charge would be at twice that distance. Height was chosen to be 0.25 m, representative of the height for the assumed blast scenario, which was 1 m for the prototype bridge. In that perspective, a scale distance, given by $Z=x/w^{0.333}$, is a relative scale distance without units, but allowing relative comparison between test cases in Table 2. Note that the smaller scale distances create larger pressure and impulse. The maximum blast charge was limited to W due to the constraints at the test site. The target deformation of the columns was achieved by changing the standoff distances.

The target deformations of the columns were set equal to 4° and 2° of rotational angle at the base of the RC column for Tests 1 and 2, respectively. These deformation limits were chosen based on recommended design limits by Mays and Smith (1995) for RC beams and slabs. The support rotations of 2° and 4° correspond to minor damage and extensive plastic hinging of the member, respectively. These rotational angles at the bottom of the column were obtained by assuming that the maximum deformation of the column occurred at the height of explosion, i.e., 0.25 m from the ground. This maximum deformation was calculated by simplified analysis using an equivalent SDOF system and energy conservation. The details of this simplified analysis will be presented in the analytical study later. The standoff distances and charge weights of Tests 3 and 4 on steel jacketed RC columns were selected to be the same as Tests 1 and 2 on RC columns, respectively.

Experimental Observations

Fig. 4 shows the photo of each column after testing, and Fig. 5 illustrates the corresponding deformation and damage of each column from side view. The posttest deformation of the column (from which residual plastic rotation can be calculated) was obtained by attaching a string at the original positions of top and bottom of the column using a measuring tape to record the dis-

Table 2. Summary of Column Test Cases and Test Observations

Test number	Column	Objective	Charge weight	Standoff distance	Charge height (m)	Relative scaled distance, Z (in $X/W^{0.333}$)	Test observations
Prototype	—	—	—	—	—	3.74	—
Test 1	RC1	$\theta=4$ deg, collapse	W	2.16 X	0.250	2.16	Shear failure at base
Test 2	RC2	$\theta=2$ deg, minor damage	W	3.25 X	0.250	3.25	Onset of shear failure at base
Test 3	SJ2	Same as Test 1	W	2.16 X	0.250	2.16	Shear failure at base
Test 4	SJ1	Same as Test 2	W	3.25 X	0.250	3.25	Shear failure at base
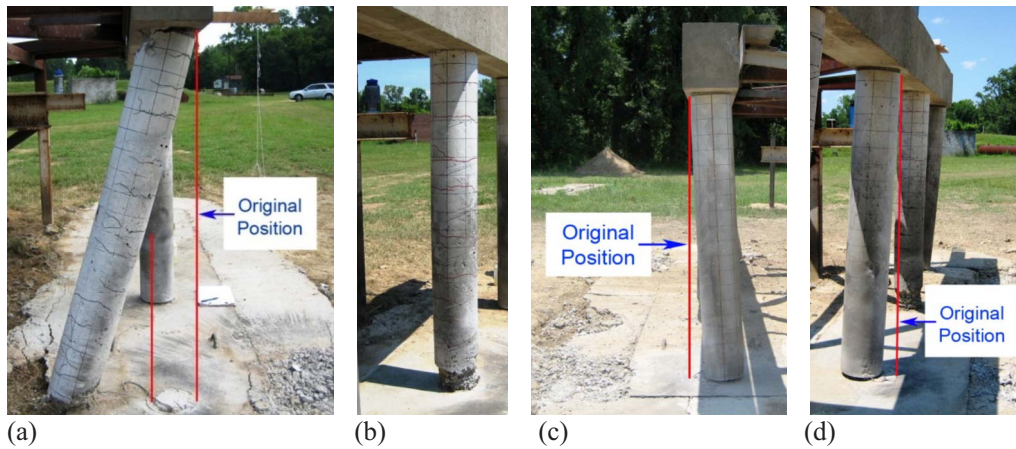
Fig. 4. Columns after tests: (a) side view of Column RC1, Test 1; (b) front diagonal view of Column RC2, Test 2; (c) side view of Column SJ2, Test 3; and (d) side view of Column SJ1, Test 4

tance to the column. In Figs. 5(a and b), crack patterns observed after tests are shown along the height of the RC columns. Column RC1 did not exhibit a ductile behavior under blast loading, but rather failed in shear at the base of the column as shown in Figs. 4(a) and 5(a). The progression of damage for Column RC1 could be explained as follows, based on observations of the column damage after the test. First, plastic hinges were deemed to form at the base of the column and at the height of the explosion, and possibly at the top of the column as well. Evidence of a plastic hinge formation around the explosion height could be seen in some cracks observed on the back side of the column as shown in Fig. 5(a). This figure also shows that the part of the column from the base up to a height of about 838 mm (33 in.) had a slight curvature outward to the back side, which agrees with the moment that would develop under this assumption. Then, while these plastic hinges were developing or after these hinges formed, the column could have been sheared off at its base because the shear force developed exceeded the direct shear strength at that location. Fig. 6(a) shows the damage of the bottom part of the column. Finally, blast pressures acting on the column and/or inertia forces developed in the column pushed the cantilever column supported from the top to rotate toward the back side. As a result, a negative moment developed at the top of the column, leading to fracture of the steel bars on the tension side at the top of the column and to spall off the cover concrete on the compression side, as shown in Fig. 6(b). Note that some sources (such as Conrath et al. 1999) indicate that direct shear failure occurs prior to any significant bending deformation of a structural member. However, if direct shear had indeed occurred prior to the development of flexural deformations in this case, then the flexural crack patterns and slight curvature of the column outward to the back side that were observed in Column RC1, for example, would be hard to explain.

The concrete spalling was observed around the bottom of Column RC2 as shown in Figs. 4(b) and 5(b). Fig. 6(c) shows the bottom of this column. The concrete cover spalled off up to a height of 117 mm (4 5/8 in.) from the base of the column. The shear deformations at the bottom part of the column can be observed by comparing against the longitudinal reinforcement vertical solid line in Fig. 5(c). Therefore, Column RC2 was deemed to exhibit the onset of direct shear failure at the base of the column. Both steel jacketed RC columns, Column SJ2 and SJ1, were sheared off from the footing surface at the concrete joint as shown

in Figs. 4(c) and 5(c) and Figs. 4(d) and 5(d), respectively. These columns were tilted toward the back side, rotating around a point at the top of the columns after the columns sheared off at their base. All the longitudinal bars at the bottom of both columns were observed to be fractured. The steel jacketed RC column remained straight and no structural damage was observed along these columns.

Analytical Study

Simplified Blast Analysis by Equivalent SDOF System

The test blast parameters previously shown in Table 2 were determined based on the calculated maximum deformations of the RC columns. These maximum deformations were obtained by simplified analysis using an equivalent SDOF system and energy conservation (see Biggs 1964 and Fujikura et al. 2007, 2008 for details). Essentially, this method considers an equivalent SDOF system having an elastic-perfectly plastic behavior, and assumes that all the energy imparted to the system by the blast loading is
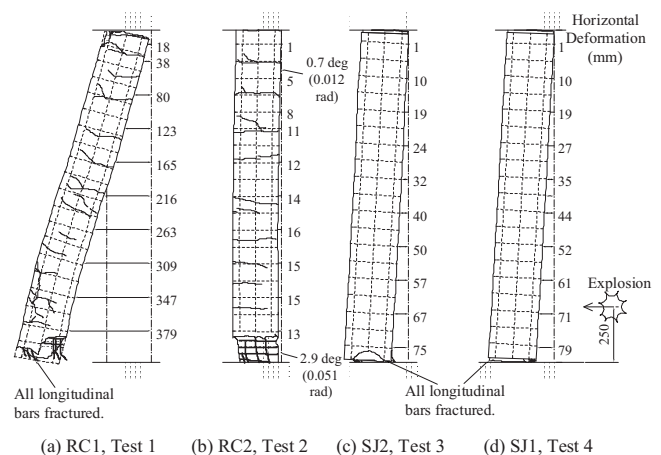
Fig. 5. Sketches of columns after tests from side view: (a) Column RC1, Test 1; (b) Column RC2, Test 2; (c) Column SJ2, Test 3; and (d) Column SJ1 Test 4
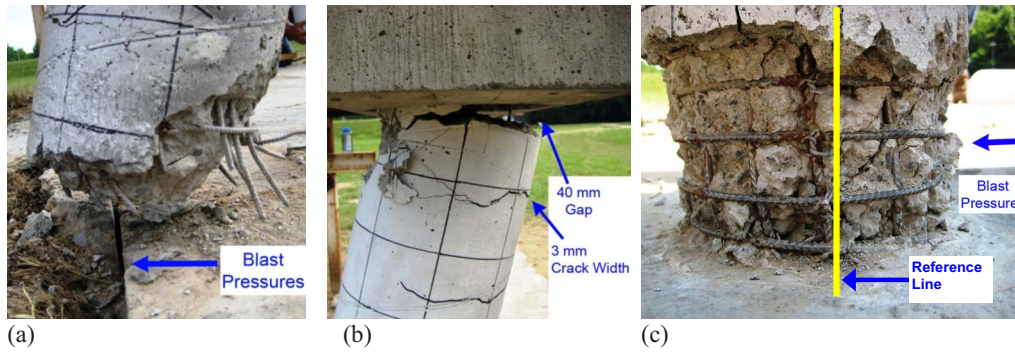
Fig. 6. Damage of RC Columns from side view: Column RC1 at (a) base; (b) top; and (c) Column RC2 at base

converted into internal strain energy. Under these conditions, the maximum deformation due to impulsive-type blast loading, X_m, is given by

$$X_m = \frac{1}{2}\left(\frac{I_{eq}^2}{K_{LM}mR_u} + X_E\right) \quad (2)$$

where I_{eq}=equivalent uniform impulse per unit length; K_{LM}=load-mass factor; m=mass per unit length of the column; R_u=strength per unit length of the column; and X_E=displacement at the onset of plastic behavior. In this analysis, I_{eq} was calculated by

$$I_{eq} = \beta D i_{eq} \quad (3)$$

where i_{eq}=equivalent uniform impulse per unit area; D=column diameter; and β=factor to account for the reduction of pressures on the circular column due to its circular shape. This factor β could be taken as 0.45. This value of 0.45 was obtained from previous blast test results of CFST columns by comparing the observed maximum deformations with the results predicted by this simplified analysis (Fujikura et al. 2007, 2008).

The magnitude of this equivalent uniform impulse per unit area, i_{eq}, in Eq. (3) was calculated by

$$i_{eq} = \frac{\displaystyle\int_0^H i(z)\delta(z)dz}{\displaystyle\int_0^H \delta(z)dz} \quad (4)$$

where $i(z)$ indicates the variation of impulse per unit area along the height of the column and $\delta(z)$=normalized deflected shape of the column. In this analysis, $i(z)$ was taken as the envelope of maximum impulse (per unit area) at any time along the height of the column. Values of $i(z)$ were calculated using the program Bridge Explosive Loading [Bridge Explosive Loading (BEL), version 1.1.0.3, U.S. Army Corps of Engineers' Engineer Research and Development Center, Vicksburg, Miss., 2004] which generates airblast pressures considering reflections of the blast wave on the ground. Also, the blast pressures applied to the cap

beam during the tests were not considered because the blast pressures were deemed to reach the cap beam after the damage of the columns. In fact, due to its greater distance to the charge, it was found from the analysis that the magnitude of the blast pressures applied to the cap beam was relatively small. Assuming that the in-span hinge develops at the height of the blast charge and both top and base of the column, the normalized deflected shape, $\delta(z)$, for inelastic deformations after plastic hinging is given as a system of rigid-link members between those plastic hinges. In other words, the deflected shape consists of two linear segments between plastic hinges, as described in Biggs (1964) for plastic response. Note that, prior blast test results for CFST columns showed that this simplified analytical method using Eqs. (2)–(4) along with β of 0.45 could predict the maximum residual deflection of the CFST column (Fujikura et al. 2007, 2008).

For the fix-fix boundary conditions and this deflected shape, the load-mass factor is K_{LM}=0.66 and r_u is given by $r_u = 28.8M_p/L^2$ where L=height of the column and M_p=plastic moment capacity of the column calculated by XTRACT as presented previously. Note that, although the rotation of the cap beam was not restrained by the reaction frame during the tests, analysis of the structural system revealed that the columns effectively had fix-fix boundary conditions because the cap beam provided a substantial rotational restraint at the top of the columns. Finally, X_E is given by $X_E = r_u/K_e$ where K_e, the unit elastic stiffness of the equivalent SDOF system, is given by $K_e = 307EI_e/L^4$. The flexural stiffness of the column, EI_e, was also calculated using XTRACT.

The results of these simplified analyses of Column RC1 for Test 1 and Column RC2 for Test 2 are summarized in Table 3 including the analytical results of peak blast pressure and maximum impulse: the maximum deformation (total elastic and plastic deformation) and plastic rotation at bottom respectively are 19.2 mm and 4.4° for Test 1 and 9.5 mm and 2.2° for Test 2. The objective of Test 1 and Test 2 were, respectively, to induce extensive plastic rotation of the column base and minor damage to the column base as presented previously. Although Column RC1 after Test 1 exhibited some level of inelastic flexural deformations, the magnitude of plastic rotation that happened before direct shear failure cannot be reliably obtained for a lack of the reference

Table 3. Summary of Simplified Blast Analysis Results of RC Tests

Test number and column	Peak blast pressure [MPa (ksi)]	Maximum impulse [MPa·ms (psi·ms)]	Equivalent uniform impulse [MPa·ms (psi·ms)]	Ultimate resistance [kN/m (kip/in.)]	Yield deformation [mm (in.)]	Maximum deformation [mm (in.)]	Plastic rotation at bottom θ (degrees)
Test 1 RC1	160.6 (23.3)	13.23 (1,917.7)	6.07 (880.7)	180 (1.03)	6.4 (1/4)	19.2 (3/4)	4.4
Test 2 RC2	82.0 (11.9)	7.22 (1,046.6)	3.81 (552.0)	180 (1.03)	6.4 (1/4)	9.5 (3/8)	2.2

point at the base of the column from the test observations. From the measured deformations of Column RC2 after Test 2, the plastic rotation at the base of this column was 2.5° (0.043 rad) calculated from the experimental residual deformation of 16 mm at a height of 370 mm from the base. This experimentally obtained rotation was larger than the prediction of 2.2° calculated by the simplified analysis because the bottom part of the column itself also deformed in shear, which was not considered in this analysis, but occurred in the experiment.

Simple Plastic Analyses

Simple plastic analyses were conducted to calculate the ultimate lateral load capacity and reactions of the RC columns and the steel jacketed RC columns. A simple plastic analysis is suitable to calculate ultimate global structural capacities. In this analysis, a rigid-perfectly plastic hinge model was assumed with a zero-length plastic hinge. A step-by-step plastic analysis was conducted, following the structural behavior from the initial elastic stage up to formation of a collapse mechanism (details of the step-by-step plastic analysis method are presented in numerous text books, such as in Bruneau et al. 1998). This simple plastic analysis could be used for these column tests because experimental observations of Column RC1 showed that plastic hinges formed at top and base of the column and around the explosion height. The blast pressures were simplified to load the column as a point load acting at the height of the blast charge. Note that this simple plastic analysis based on the maximum capacity developed in a cross section is a procedure consistent with what most blast-resistant design guidelines advocate for shear design. It also has the advantage of not being dependent upon the precise sequence of response mechanisms that occur because it considers the maximum demand that can develop in a section based upon the governing flexural capacity—an approach that should be familiar to practicing engineers.

The plastic hinges were assumed to develop at the height of the blast charge and both at the top and base of the column. By using XTRACT, the plastic moment capacity of RC column sections was taken as 14.0 kN·m (124.0 kip·in.), and that of steel jacketed RC columns was taken as 15.2 kN·m (134.6 kip·in.) at both top and base and 34.5 kN·m (305.0 kip·in.) at the explosion height (steel jacket considered to act compositely at that section). In the analyses, applied forces, reactions at both top and base of the column and deflections at the load point were calculated in each step and are plotted in Figs. 7(a and b) for RC column and steel jacketed RC column, respectively. The maximum resulting reaction forces at the base and top were 112.1 kN (25.2 kip) and 22.4 kN (5.0 kip), respectively, for RC column, and 198.7 kN (44.7 kip) and 39.7 kN (8.9 kip), respectively, for steel jacketed RC column.

Direct Shear Resistance of Test Column

Direct shear resistance of the test columns was compared with the reaction forces calculated by simple plastic analyses. Direct shear resistance of reinforced concrete sections, V_n, was calculated using the "modified shear-friction method" strength equation (ACI 2004) given by

$$V_n = 0.8A_{vf}f_yD_{sy} + A_cK_1D_c \qquad (5)$$

where A_{vf}=area of shear-friction reinforcement across shear plane; f_y=yield strength of reinforcement; A_c=area of the concrete section resisting shear transfer; and K_1=2.8 MPa (400 psi)
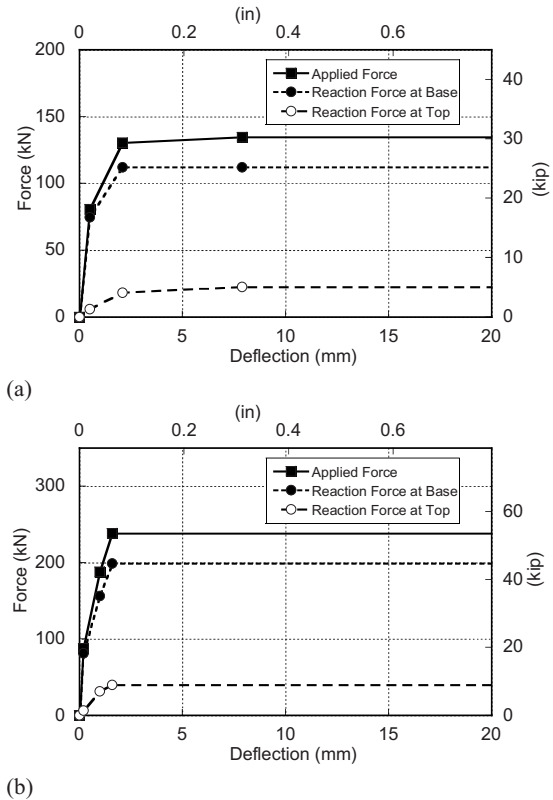

Fig. 7. History of load versus deflection at load point: (a) RC column; (b) steel jacketed RC column

for normal weight concrete. D_{sy} and D_c are, respectively, the dynamic increase factors for yield stress of steel and for concrete compressive strength. Note that the effect of dynamic loading was considered by incorporating the strain rate effect on material properties into this equation through these dynamic increase factors. Some sources (such as USDA 1990) suggest D_{sy} and D_c to be 1.1 to account for uncertainties in the design process for shear. However, for the purpose of replicating the experimental behaviors and remove this conservatism introduced for the design purposes, D_{sy} and D_c were taken as 1.2 and 1.25, respectively (Mays and Smith 1995), which are the same dynamic increase factors as for bending.

Because the RC column section and the steel jacketed RC column section at their base had the same configuration and materials, these columns were calculated to have the same direct shear resistance as given by Eq. (5). For A_{vf}=309.6 mm², f_y =501 MPa, A_c=32,365 mm², and K_1=2.8 MPa, the direct shear resistance, V_n, of the tested columns is 262.2 kN (58.9 kip). This resistance is larger than the maximum reaction forces at the base of the columns calculated by the simple plastic analyses, namely 112.1 and 198.7 kN for the RC column and the steel jacketed RC column, respectively. This calculation indicated that those columns would not fail in direct shear at their base. However three of the test columns were found to fail in direct shear at their base during the experiments.

To explain the direct shear behavior observed in the tests, it was decided to investigate the possible reduction of direct shear strength in a plastic hinge region. When a large bending moment is applied at the reinforced concrete section, cracking occurs in the tension zone of the concrete section. At this point, flexure is resisted by the compression zone of the section and the steel
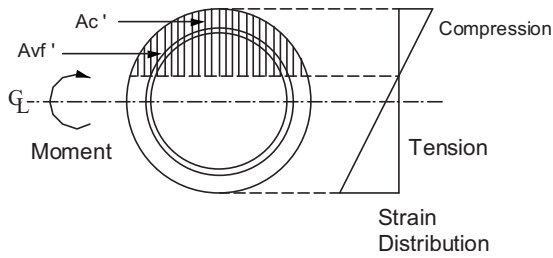
Fig. 8. RC column under bending moment

(a)

(b)

Fig. 9. Comparison of shear resistance with shear force at base of (a) RC column; (b) steel jacketed RC column

reinforcement in the tension zone of the section. Direct shear resistance given by Eq. (5) is the sum of the cohesion and friction resistance along the direct shear interface. In this calculation, the parts on both sides of the direct shear interface fully contact each other. However, on a cracked section under bending moment, contact can only exist in the compression zone of the section. This is particularly the case in regions of plastic hinging. Therefore, because (as observed experimentally and also indicated from simple plastic analyses) a plastic moment developed at the base of the column, the above was considered to develop a moment-direct shear interaction model. For this model, only the part of the section in compression is assumed to be able to resist the shear force, since direct shear resistance is deemed unable to develop when two surfaces do not contact each other. The contribution of the longitudinal reinforcement to the direct shear resistance is not included in this model because its contribution is considered to be small under the high longitudinal strains in the steel bars due to the large moment.

Fig. 8 schematically shows a reinforced concrete section subjected to a bending moment used to formulate the moment-direct shear interaction model. This model is based on plane section analysis (assuming that plane sections remained plane when subjected to bending). The part of the section hatched in Fig. 8 is in compression. By replacing A_{vf} and A_c in Eq. (5) with A'_{vf} and A'_c, respectively, the modified direct shear resistance, V'_n, is given by

$$V'_n = 0.8A'_{vf}f_yD_{sy} + A'_cK_1D_c \qquad (6)$$

where A'_{vf} and A'_c = area of longitudinal reinforcement and concrete in the compression zone as shown in Fig. 8. The position of the neutral axis needs to be determined to calculate this compression zone. This neutral axis position was calculated by moment-curvature analysis using XTRACT.

Figs. 9(a and b) compares the new direct shear resistance at the base of the columns calculated per the above modified procedure with the shear force developed at the base of RC columns and steel jacketed RC columns, respectively, varying as a function of the moment developed at their base. These direct shear resistance were calculated by Eq. (6), and the shear forces were obtained from the simple plastic analyses. A solid curve with open circles and a dashed line represent the direct shear resistance and the shear force developed, respectively, in these figures. For the direct shear resistance curve, the second y-axis presents the ratio of V'_n to V_n which shows the reduction of direct shear resistance due to the moment applied at the section.

The solid lines in Figs. 9(a and b) show that for both columns, as the moment increases, the direct shear resistance (capacity of columns) decreases due to the shift of the neutral axis position toward the outer compression fiber. Obviously, a larger shear force demand develops at the column base as the moment increases due to the increase of the applied load as shown by the dashed curves in these figures, and a first plastic hinge would
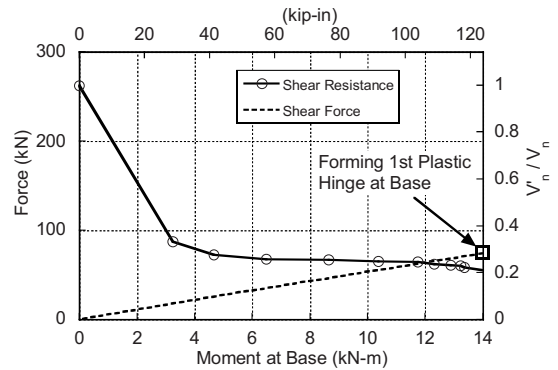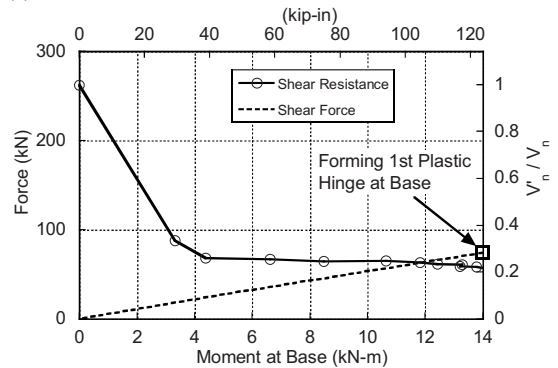
develop at the base of the column (in absence of other governing limit states) when the applied force equals 80.7 kN (18.1 kip) for RC columns and 87.6 kN (19.7 kip) for steel jacketed columns. The intersection of these curves is the point where the shear force is equal to the direct shear resistance and, when this happens before plastic flexural hinging can develop (as is the case in Fig. 9), direct shear failure would occur. This point occurs at shear force of 63.0 kN (14.2 kip) and corresponding moment of 11.8 kN·m (104.5 kip·in.) for the RC column, and shear force of 63.6 kN (14.3 kip) and corresponding moment of 11.9 kN·m (105.5 kip·in.) for the steel jacketed RC column. Figs. 9(a and b) also show that direct shear failure was deemed to occur in both columns before the first plastic hinge develops at the base of the columns. According to these results, it appears that this moment-direct shear interaction model correctly allows to capture the experimentally observed behavior. Note that this moment-direct shear interaction model is to be compared with static shear force developed from the simple plastic mechanism.

Conclusions

Standard seismically detailed ductile RC columns, and nonductile RC columns retrofitted with steel jackets to become ductile, were not found to exhibit a ductile behavior under blast loading, and failed in direct shear at their base rather than by flexural yielding (for comparison, similar CFST columns subjected to similar or greater blast forces failed in a ductile manner). Reinforced concrete details by current seismic codes, and steel jacketing, known to be effective to provide satisfactory seismic performance, were thus shown to be ineffective for the blast loading cases considered. A moment-direct shear interaction model to calculate the

direct shear resistance of RC sections was proposed to account for the reduction of direct shear resistance on cross sections simultaneously subjected to large moments.

Future Research

Future research could investigate the effect of axial force on the observed behavior of columns under blast loading, and additional data points to establish the impact of axial force on direct shear resistance. Detailed three-dimensional finite element models could be developed to further investigate the behavior of the column types tested, and to model development of the direct shear failure at the base of these columns. Future research is also desirable to investigate means and methods to prevent direct shear failure at the base of reinforced concrete columns and steel jacketed reinforced concrete columns subjected to blast loads.

Acknowledgments

References

AASHTO. (2004). *AASHTO LRFD bridge design specifications*, 3rd Ed., Washington, D.C.

Agrawal, A. K., Alampalli, S., and Ettouney, M. (2009). *Workshop on Safety and Behavior of Bridges Subjected to Blast in a Multi-Hazard Environment*, New York.

American Concrete Institute (ACI). (2004). *Building code requirements for structural concrete (ACI 318-05) and commentary (ACI 318R-05)*, Farmington Hills, Mich.

Anwarul Islam, A. K. M., and Yazdani, N. (2006). "Blast capacity and protection of AASHTO girder bridges." *Proc., 4th Forensic Congress*, ASCE, Reston, Va.

ASCE. (2008). *Proc., Bridge Workshop—Enhancing Bridge Performance*, ASCE, Reston, Va.

Biggs, J. M. (1964). *Introduction to structural dynamics*, McGraw-Hill, New York.

Bruneau, M., Uang, C. M., and Whittaker, A. (1998). *Ductile design of steel structures*, McGraw-Hill, New York.

Buckle, I. G., Friedland, I., Mander, J., Martin, G., Nutt, R., and Power, M. (2006). *Seismic retrofitting manual for highway structures: Part 1—Bridges, MCEER-06-SP10*, MCEER, Buffalo, N.Y.

California Department of Transportation (CALTRANS). (2003). *Bridge design specifications*, Sacramento, Calif.

California Department of Transportation (CALTRANS). (2006). *Seismic design criteria. Version 1.4*, Sacramento, Calif.

Chai, Y. H., Priestley, M. J. N., and Seible, F. (1991). "Flexural retrofit of circular reinforced concrete bridge columns by steel jackets." *Rep. No. SSRP-91/06*, Dept. of Applied Mechanics and Engineering Sciences, Univ. of California, San Diego.

Conrath, E. J., Krauthammer, T., Marchand, K. A., and Mlakar, P. F. (1999). *Structural design for physical security: State of the practice*, ASCE, Reston, Va.

Davis, C. E., Williams, G. D., Williamson, E. B., Marchand, K. A., McKay, A. E., and Bayrak, O. (2009). "Design and detailing guidelines for bridge columns subjected to blast and other extreme loads." *Proc., 2009 Structures Congress*, ASCE, Reston, Va.

Federal Highway Administration (FHWA). (2003). "Recommendations for bridge and tunnel security." *Rep. Prepared by the Blue Ribbon Panel on Bridge and Tunnel Security*, Washington, D.C.

Fujikura, S., and Bruneau, M. (2008). "Experimental and analytical investigation of blast performance of seismically resistant bridge piers." *Technical Rep. MCEER-08-0028*, MCEER, Univ. at Buffalo, Buffalo, N.Y.

Fujikura, S., Bruneau, M., and Lopez-Garcia, D. (2007). "Experimental investigation of blast performance of seismically resistant concrete-filled steel tube bridge piers." *Technical Rep. MCEER-07-0005*, MCEER, Univ. at Buffalo, Buffalo, N.Y.

Fujikura, S., Bruneau, M., and Lopez-Garcia, D. (2008). "Experimental investigation of multihazard resistant bridge piers having concrete-filled steel tube under blast loading." *J. Bridge Eng.*, 13(6), 586–594.

Jenkins, B. M. (2001). "Protecting public surface transportation against terrorism and serious crime: Continuing research on best security practices." *MTI Rep. No. 01-07*, Mineta Transportation Institute, San Jose, Calif.

Mander, J. B., Priestley, M. J. N., and Park, R. (1988). "Theoretical stress-strain model for confined concrete columns." *J. Struct. Eng.*, 114(8), 1804–1826.

Marson, J., and Bruneau, M. (2004). "Cyclic testing of concrete-filled circular steel bridge piers having encased fixed-based detail." *J. Bridge Eng.*, 9(1), 14–23.

Mays, G. C., and Smith, P. D. (1995). *Blast effects on buildings*, Telford, London.

MCEER/ATC-49. (2003). *Recommended LRFD guidelines for the seismic design of highway bridges, Part I: Specifications and II: Commentary and appendices*, Buffalo, N.Y.

Priestley, M. J. N., Seible, F., and Calvi, G. M. (1996). *Seismic design and retrofit of bridges*, Wiley, New York.

Ray, J. C. (2006). "Validation of numerical modeling and analysis of steel bridge towers subjected to blast loadings." *Proc., 2006 Structures Congress*, ASCE, Reston, Va.

USDA. (1990). "Structures to resist the effects of accidental explosions." *Technical manual TM 5-1300*, Washington, D.C.

Williamson, E., and Williams, D. (2009). "Prediction of airblast loads on bridge columns." *Proc., 80th Shock & Vibration Symp.*, SAVIAC, San Diego.

Winget, D. G., Williamson, E., Marchand, K. A., and Gannon, J. C. (2008). "Recommendations for blast design and retrofit of typical highway bridges." *J. Transportation Research Board*, CD 11–S.

Yi, Z. (2009). "Blast load effects on highway bridges." Ph.D. dissertation, The City Univ. of New York, New York.